

# Quantum algorithms for phase space tomography

Juan Pablo Paz,<sup>1,2,\*</sup> Augusto José Roncaglia,<sup>1,2,†</sup> and Marcos Saraceno<sup>3,‡</sup>

<sup>1</sup>*Departamento de Física, FCEyN, UBA, Pabellón 1,  
Ciudad Universitaria, 1428 Buenos Aires, Argentina*

<sup>2</sup>*Theoretical Division, LANL, MSB213, Los Alamos, NM 87545, USA*

<sup>3</sup>*Unidad de Actividad Física, Tandara, CNEA, Buenos Aires, Argentina*

(Dated: June 22, 2021)

We present efficient circuits that can be used for the phase space tomography of quantum states. The circuits evaluate individual values or selected averages of the Wigner, Kirkwood and Husimi distributions. These quantum gate arrays can be programmed by initializing appropriate computational states. The Husimi circuit relies on a subroutine that is also interesting in its own right: the efficient preparation of a coherent state, which is the ground state of the Harper Hamiltonian.

PACS numbers: 03.67.Lx, 03.65.Wj

## I. INTRODUCTION

Phase space distributions have been used as representation tools for quantum mechanical operators since the early days of quantum mechanics. They provide the ideal link to explore and understand the transition to classical mechanics and to display in phase space quantum effects. Their properties are very well known [1, 2] when the phase space is  $\mathbb{R}^2$ . For systems with a finite dimensional space of states the distributions become discrete, i.e. they are defined over a finite lattice [3, 4]. Discrete phase space distributions have been used in the context of studies of quantum maps on bounded phase space [5, 6] and they have also recently proposed as a useful tool for studies related to quantum information and computation [7, 8, 9]. The simplest way to characterize them, for a Hilbert space of dim  $N$  is by using a complete basis of  $N^2$  operators  $\{\Lambda_\alpha; \alpha = 0, \dots, N^2 - 1\}$ , in terms of which the distribution is given as  $\text{Tr}[\Lambda_\alpha^\dagger \rho]$ . The properties and classical features that these distributions display depend of course on the operator basis  $\{\Lambda_\alpha\}$ . In this sense phase space distributions are nothing but the coefficients of the expansion of the state  $\rho$  in the basis  $\Lambda_\alpha$ . The determination of the value of  $\text{Tr}[\Lambda_\alpha \rho]$  for every  $\alpha$  is, thus, a particular form of quantum state tomography (see [10] and references therein).

In a recent paper [11] it was shown how to efficiently measure the discrete Wigner function at any phase space point. The basis of the method is the use of the so-called 'scattering circuit' to efficiently determine the value of the quantity  $\text{Tr}[\rho A]$  provided that the operation  $A$  can be implemented in a controlled way. Thus, if the complete basis  $\Lambda_\alpha$  consists of unitary operators then the scattering circuit can be used to measure individual values of the distribution. The disadvantage is of this approach is that, as  $\alpha$  enters as a classical parameter, a new gate

array has to be applied for each  $\alpha$ . In this paper we will extend the results presented in [9, 11] in two ways. First, we will show how to efficiently measure other phase space distribution functions (Husimi, Kirkwood). Second, we will show how to do this by using quantum circuits with a fixed architecture, which is independent of the phase space point  $\alpha$ . These circuits belong to the class of programmable quantum devices, whose action is controlled by quantum software, that have been under investigation recently [12, 13]. In this paper we will show how to build efficient programmable circuits to measure three phase space distributions: Wigner, Kirkwood and Husimi. It is also worth mentioning here that the quantum circuits we developed use a subroutine which is interesting in its own right and could be useful for other applications. In fact, in this paper we present a method to efficiently prepare coherent states (which are rigorously defined below, but can be roughly characterized as approximately Gaussian wave packets obeying periodic boundary conditions).

The paper is organized as follows in Section II we present the circuit that enables the programmable measurement of the discrete Wigner function. We also show that it can be useful to compute averages of this function over various phase space domains (this extends and completes results presented in [13]). In Section III we present a simple programmable circuit that evaluates the Kirkwood distribution at any phase space point. In Section IV we present the quantum gate array that efficiently evaluates the discrete Husimi distribution. This gate uses coherent states as inputs. The algorithm to efficiently prepare those states is presented in Section V. Finally, we present some conclusions in Section VI.

## II. PROGRAMMABLE TOMOGRAPHY OF THE DISCRETE WIGNER FUNCTION

The discrete Wigner function [9, 11] in a Hilbert space of dimension  $N$  is defined in terms of the basis of phase point unitary operators:

$$A(q, p) = U^q R V^{-p} e^{i \frac{p}{N} q}, \quad (1)$$

\*Electronic address: jpaz@lanl.gov

†Electronic address: augusto@lanl.gov

‡Electronic address: saraceno@tandar.cnea.gov.ar

as

$$W(q, p) = \frac{1}{2N} \text{Tr}[A(q, p)\rho] \quad (2)$$

where  $q, p$  are integer labels spanning a grid of size  $2N \times 2N$ .  $U$  and  $V$  are respectively the translation operators in the  $|q\rangle$  and  $|p\rangle$  basis ( $U|q\rangle = |q+1\rangle$ ,  $U|p\rangle = e^{-i\frac{2\pi}{N}p}|p\rangle$ ,  $V|p\rangle = |p+1\rangle$ ,  $V|q\rangle = e^{i\frac{2\pi}{N}q}|q\rangle$ ), which are related by the discrete Fourier transform.  $R$  is the reflection operator ( $R|n\rangle = |N-n\rangle$ ). Only an  $N \times N$  sub-grid is needed for the complete tomography of the state (but the larger grid is required to define a Wigner function with all the desired properties [9]).

The programmable circuit implementing the measurement of the discrete Wigner function is shown in Figure 1. This was introduced in [13] as a particular case of a programmable circuit evaluating the expectation value of an arbitrary operator. It is a variation of the so-called scattering circuit [11] where an ancillary qubit acts as a probe for a more complex system with which it interacts by means of controlled operations. The circuit shown in Figure 1 has several registers: The first register is an ancillary qubit (the probe) initially prepared in the state  $|0\rangle$  which is an eigenstate of  $\sigma_z$  with eigenvalue  $+1$ . The following two registers act as program registers and should be prepared in the state  $|q\rangle|p\rangle$ . The last register stores the state of the system of interest  $\rho$ . The program state contains the information about the binary expansion of the coordinates of the point in the phase space where we wish evaluate the Wigner function. As seen in the circuit, the role of the program states is to control the application of displacement operators on the system register. Here, and in what follows, we use the convention that for any operator  $O$ , “controlled- $O$ ” operators act as:  $(\text{ctrl-}O)|n\rangle|\Psi\rangle = |n\rangle O^n|\Psi\rangle$ . In particular, in Figure 1 an operator such as “control- $V_{2N}$ ” acts as  $(\text{ctrl-}V_{2N})|q\rangle|p\rangle = |q\rangle V_{2N}^q|p\rangle = e^{i\frac{2\pi}{N}pq}|q\rangle|p\rangle$  (note that a subscript in any operator indicates the dimensionality of the space in which it acts). It is straightforward to show that the final polarization of the ancillary qubit turns out to be:

$$\langle\sigma_z\rangle = 2N\text{Tr}[A(q, p)\rho] = 2NW(q, p). \quad (3)$$

### A. Measuring the sum of the discrete Wigner function over domains in phase space

One of the defining properties of the Wigner function is the fact that adding its values over lines in phase space one always obtains the probability to measure an observable. It is interesting to notice that the circuit shown in Figure 1 can be programmed to directly evaluate the average of the Wigner function along any line in phase space. More generally, the state of the program register can be used to define the phase space domain over which the Wigner function is averaged.

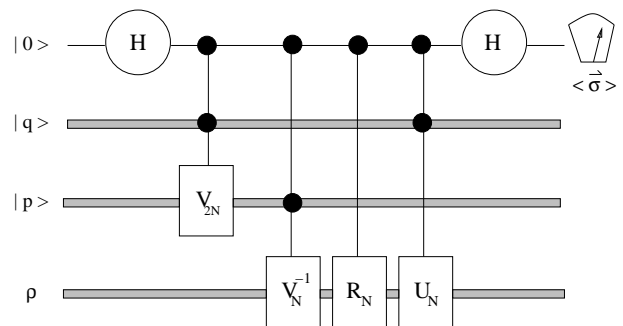


FIG. 1: Programmable circuit to evaluate the discrete Wigner function from the polarization of the first qubit. The second and the third registers store the information about the the phase space point where the distribution is being measured. All states are initialized in the computational (coordinate) basis. All “ctrl- $O$ ” operations act as  $(\text{ctrl-}O)|n\rangle|\Psi\rangle = |n\rangle O^n|\Psi\rangle$ . A subscript in an operator denotes the dimension of the space in which it acts. In all figures we adopt the following graphic convention: thin cables denote a single qubit, and wide cables denote systems of more than one qubit.

Let us consider first the case of lines. The quantity in which we are interested is  $\sum_{(q,p)\in L} W(q, p)$ , the sum of the values of the Wigner function along the line  $L$ . It is easy to see that for the program state  $|\Psi\rangle_P = \sum_{p=0}^{2N-1} |n_3\rangle \otimes |p\rangle / \sqrt{N}$ , the final polarization turns out to be  $\langle\sigma_z\rangle = \sum_p W(n_3, p)$ . As this type of program state can be efficiently constructed, the example shows that it is possible to estimate the sum of the values of the Wigner function along vertical and horizontal lines. In a recent work [13] we showed that this is a special case of a more general result that establishes the possibility to program the measurement of the expectation value of any operator. Following the same idea, consider the program state

$$|\Psi\rangle_P = \frac{1}{K} \sum_{(q',p')\in L} |q'\rangle|p'\rangle \quad (4)$$

where  $L : n_1q + n_2p = n_3$ ,  $0 \leq n_i \leq 2N - 1$  and  $K$  is a normalization constant (the square root of the number of points in the line  $L$ ). Then, the final polarization is:

$$\langle\sigma_z\rangle = \frac{2N}{K^2} \sum_{(q',p')\in L} W(q', p'). \quad (5)$$

This is precisely the quantity we are interested in. However, the above program states may be difficult to prepare (they are, in general, highly entangled states). To avoid using program states which may be difficult to prepare we have developed an alternative method. This was briefly described in [13]. For completeness, we present it here in more detail.

For our method it is convenient to employ the fact that certain unitary operators induce a purely classical transformation of the Wigner function (this means that

the Wigner function is simply transported by a canonical, area preserving, flow). This is the case for unitary operators that quantize linear canonical transformations on the torus (the so called cat maps [9]). We can use this fact as follows: First, we can prepare a simple program state that would produce the measurement of the Wigner function along vertical or horizontal lines. Then, we can obtain the corresponding measurement along tilted lines by applying the appropriate unitary cat map to the initial state. The two-parameter family of cat operators that we will use is given by:

$$U_{cat} = \mathcal{V}_b \mathcal{T} \mathcal{V}_a, \quad (6)$$

where  $a$  and  $b$  are integers, and the operators  $\mathcal{V}_a$  and  $\mathcal{T}$  are diagonal in the position and momentum basis respectively,

$$\begin{aligned} \mathcal{V}_a |n\rangle &= \exp(-i2\pi n^2(1-a)/2N) |n\rangle \\ \mathcal{T} |k\rangle &= \exp(-i2\pi k^2/2N) |k\rangle. \end{aligned} \quad (7)$$

The classical equations of motion corresponding to this system are

$$q = bq' + p' \quad p = (ab - 1)q' + ap'. \quad (8)$$

As the Wigner function evolves classically, when the phase space points are related as above, we can write  $W(q, p, t+1) = W(q', p', t)$ . The transformation (8) maps vertical lines into tilted lines according to the values of the parameters  $a$  and  $b$ . With this in mind we can try to find the linear transformation that maps a line  $L$ , whose program state is difficult to prepare, into a line  $L'$ , whose program state is easy to prepare. If we achieve this, we can compute the average Wigner function along  $L$  by using the fact that

$$\sum_{(q,p) \in L} W_\rho(q, p) = \sum_{(q',p') \in L'} W_{U_{cat} \rho U_{cat}^\dagger}(q', p').$$

The circuit to implement this procedure is shown in Figure 2. In order to implement the  $U_{cat}$  evolution, we only need to know how to apply the unitary operator  $\mathcal{T}$  and its powers. As it was shown in [15] this can be done efficiently. Taking into account that the parameters defining the evolution  $U_{cat}$  depend on the line, this network is not completely programmable (its architecture depends on each line), but we can easily prove that the device can be transformed into a fully programmable one by adding two registers specifying the values of the constants  $a$  and  $b$ .

Let us now address the issue of how to find the parameters  $a$  and  $b$  entering in (8) mapping line  $L$  and  $L'$ . For this, we consider the lines defined as

$$\begin{aligned} L &: n_1 q + n_2 p = n_3 \pmod{2N} \\ L' &: q' + p' = n_3 \pmod{2N}. \end{aligned}$$

For simplicity, we consider the case where at least one of the parameters  $n_i$  is an odd number (the other case

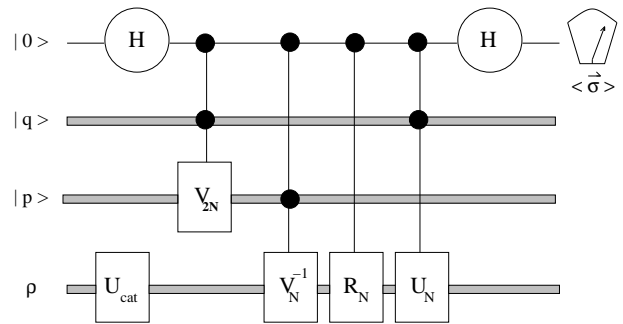


FIG. 2: Programmable gate array to evaluate the average Wigner function over a tilted line in phase space. The cat map is parameterized by two integers, which can be programmed in auxiliary registers (so the array can be made fully programmable).

can be treated similarly). It is worth mentioning that the program state for  $L'$  can be efficiently prepared. The mapping between the two lines is accomplished by using a cat map as in (8) with the parameters given by

$$\begin{aligned} n_2 a &= 1 - n_1 \pmod{2N} \\ b &= 1 + n_2 \pmod{2N}. \end{aligned} \quad (9)$$

This method can be generalized to evaluate the average value of the Wigner function over tilted rectangular regions. For this purpose, we can construct the program state for a simple rectangular region (defined by the conditions:  $q_1 \leq q \leq q_2$ ,  $p_1 \leq p \leq p_2$ ). Then, we can map this region into a tilted region by using the strategy described above.

### III. PROGRAMMABLE TOMOGRAPHY OF THE KIRKWOOD DISTRIBUTION

The Kirkwood function is a phase space distribution whose use is probably less common. It was first proposed by Kirkwood [14], and used in quantum statistics. It displays different phase space features of a quantum state in phase space and has the advantage of being directly linked to the matrix elements of the density matrix in a mixed representation. On the other hand the Kirkwood function is a complex number even for hermitian operators. Having defined the unitary basis of operators  $\{ \frac{|q\rangle\langle p|}{\langle p|q\rangle}; q, p = 0, \dots, N-1 \}$  in a Hilbert space of  $\dim N$ , the discrete Kirkwood function of a density operator  $\rho$  is defined as:

$$K(q, p) = \frac{1}{N} \text{Tr} \left[ \frac{|q\rangle\langle p|}{\langle p|q\rangle} \rho \right] \quad (10)$$

where  $|q\rangle$  and  $|p\rangle$  are position and momentum eigenstates, respectively. The circuit that implements the measurement of the Kirkwood distribution is also based on the scattering circuit. It can be seen in Figure 3, where the swap gate acts as  $S[|\Psi\rangle_1|\Phi\rangle_2] = |\Phi\rangle_1|\Psi\rangle_2$ . It

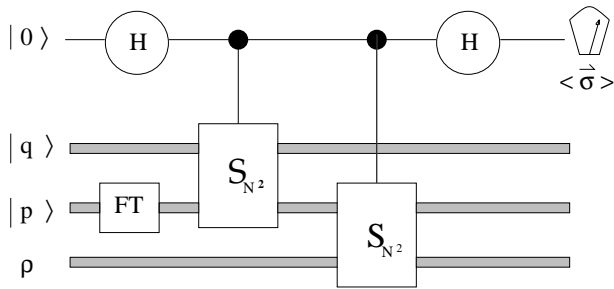


FIG. 3: Programmable gate array to measure the Kirkwood function. The first register is the ancillary (probe) qubit, the second and the third registers are the program states. The  $FT$  gate is the quantum Fourier transform, and the swap gate acts as  $S[|\Psi\rangle_1|\Phi\rangle_2] = |\Phi\rangle_1|\Psi\rangle_2$ .

is simple to show that if the program state (second and third registers) are computational states specifying the position and momentum coordinates, this circuit allows to measure the Kirkwood distribution at any point of the phase space. By measuring the expectation values of  $\langle\sigma_z\rangle$  and  $\langle\sigma_y\rangle$  for the ancillary qubit we obtain the Kirkwood distribution as

$$\langle\sigma_z\rangle - i\langle\sigma_y\rangle = \text{Tr}\left[|p\rangle\langle p|\rho|q\rangle\langle q|\right] = K(q, p). \quad (11)$$

#### IV. PROGRAMMABLE TOMOGRAPHY OF THE HUSIMI DISTRIBUTION

The Husimi function is a well known alternative distribution in phase space, which is based on the use of minimum uncertainty wave packets  $|\alpha\rangle$ . The Husimi distribution is the expectation value of the density matrix in the coherent state  $|\alpha\rangle$ . This is a positive quantity that, in the continuous case, graphically displays the phase space contents of the state in a region of area  $h$ . In the discrete case the coherent states can also be defined [16] (we provide below an efficient scheme for their preparation). These wave packets define an over-complete basis  $\{|\alpha\rangle, \alpha = (q, p), q, p = 0, \dots, N-1\}$ . In terms of this basis the Husimi distribution is defined as

$$H(\alpha) = \frac{1}{N} \text{Tr}\left[|\alpha\rangle\langle\alpha|\rho\right]. \quad (12)$$

The programmable circuit that implements the measurement of the Husimi distribution is also based on the scattering circuit (in particular, it is a straightforward application of the ideas proposed in [17] and used in the experiment presented in [18]). In Figure 4 we can see a representation of the algorithm, which uses an ancillary (probe) qubit, and a program register prepared in the state  $|\alpha\rangle$  (a coherent state centered at the point where we want to evaluate the Husimi distribution). It is easy to show that the circuit is such that

$$\langle\sigma_z\rangle = \text{Tr}\left[|\alpha\rangle\langle\alpha|\rho\right] = NH(\alpha). \quad (13)$$

The algorithm would only be useful if an efficient method can be devised to prepare the state  $|\alpha\rangle$ . We devote the next section to a complete description of this subroutine.

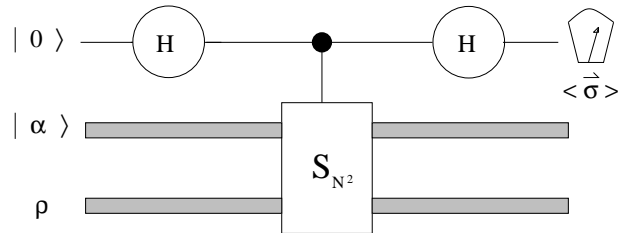


FIG. 4: Programmable circuit to measure the Husimi distribution function. The first register is the ancillary (probe) qubit, the second register is the program state (a coherent state centered at the point of interest in phase space) and the third one is the system of interest.

### V. EFFICIENT ALGORITHM FOR THE GENERATION OF COHERENT STATES

#### A. Discrete coherent states

In the continuous case, coherent states can be defined as phase space translations acting on the ground state of the harmonic oscillator Hamiltonian. In the discrete case with periodic boundary conditions, the harmonic oscillator can be replaced by the Harper Hamiltonian:

$$\left(2 - \frac{U + U^\dagger}{2} - \frac{V + V^\dagger}{2}\right)|\Phi_0\rangle = E_0|\Phi_0\rangle, \quad (14)$$

which ensures the proper periodicity conditions. Coherent states can now be defined [16] as discrete translations on  $|\Phi_0\rangle$

$$|\alpha\rangle = T(\alpha)|\Phi_0\rangle, \quad (15)$$

where  $T(\alpha) = U^q V^p e^{\frac{i\pi}{N}pq}$  are the phase space translation operators. An alternative definition, yielding a *continuous* distribution with analytic properties [19] is given by:

$$|q, p\rangle_c = \sqrt{\frac{2}{N}} e^{\frac{\pi}{2N}[q^2 + p^2]} \sum_{n=0}^{N-1} \sum_{j=-\infty}^{\infty} e^{-\frac{\pi}{N}(Nj - q + n)^2} e^{-i\frac{2\pi}{N}p(Nj + \frac{q}{2} - n)} |n\rangle. \quad (16)$$

These states are almost indistinguishable from (15) as  $N$  grows, and both are periodic wave packets occupying a minimum uncertainty area  $1/N$  in phase space. Their detailed structure, showing the extremely small differences at small values is shown in Figure 5.

The classical analogue of the Harper Hamiltonian (14) is  $H = \frac{1}{2}(\sin^2 \pi Q + \sin^2 \pi P)$ . This gives rise to the following classical map equations (for a small time step  $\gamma/2\pi$ )

$$Q' = Q - \gamma \sin(2\pi P) \pmod{1} \quad (17)$$

$$P' = P + \gamma \sin(2\pi Q') \pmod{1}. \quad (18)$$

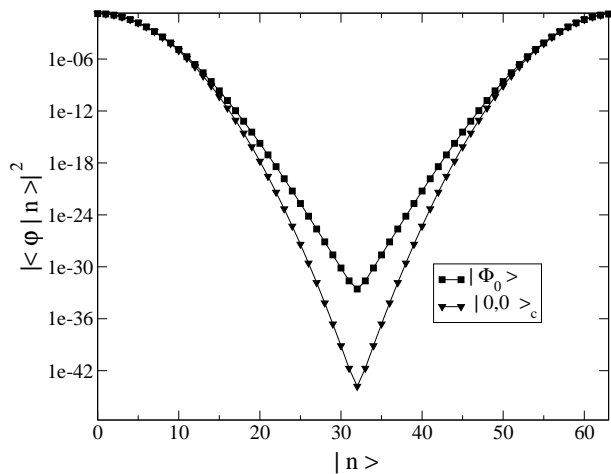


FIG. 5: Population (in the coordinate basis) of both the continuous (16) and the discrete (14) coherent states, centered at the origin of the phase space. The difference between both definitions tends to zero in the large  $N$  limit (here,  $N = 64$ ).

For infinitesimal  $\gamma$  we obtain Hamilton equations, and the conservation of energy leads to integrable behavior. Our strategy will be to quantize the map equation for small  $\gamma$  as a way to obtain a unitary operator with an eigenstate very close to  $|\Phi_0\rangle$ . The map belongs to the well known family of the kicked maps and the unitary operator corresponding to its quantization is obtained as a product of two operators representing a potential and a kinetic kick. These two operators are respectively diagonal in position and momentum basis. They can be efficiently implemented by means of a quantum network consisting of two controlled phases interposed by the Fourier transform:

$$\mathcal{U}(\gamma) = M[FT]^\dagger K[FT], \quad (19)$$

where  $FT$  is the  $N$ -dimensional Fourier transform and the operators  $M$  and  $K$  represent the potential and kinetic kicks respectively:

$$M|q\rangle = e^{-i\gamma N \cos(\frac{2\pi}{N}q)}|q\rangle \quad (20)$$

$$K|p\rangle = e^{-i\gamma N \cos(\frac{2\pi}{N}p)}|p\rangle. \quad (21)$$

The crucial feature of this unitary operator is that as  $\gamma \ll 1$  its eigenstates become those of Harper Hamiltonian. Hence,  $\mathcal{U}(\gamma)$  has a coherent state as one of its eigenstates for small values of  $\gamma$ . In Figure 6 we show how the eigenstate of the map (19) converges to the ground state  $|\Phi_0\rangle$  as  $\gamma \rightarrow 0$ .

From the above discussion is clear that what we need is a method to efficiently prepare an eigenstate of the unitary operator (19). For this, we will use the well known phase estimation algorithm [20, 21, 22] to filter an initial state which is approximately localized near the phase space origin.

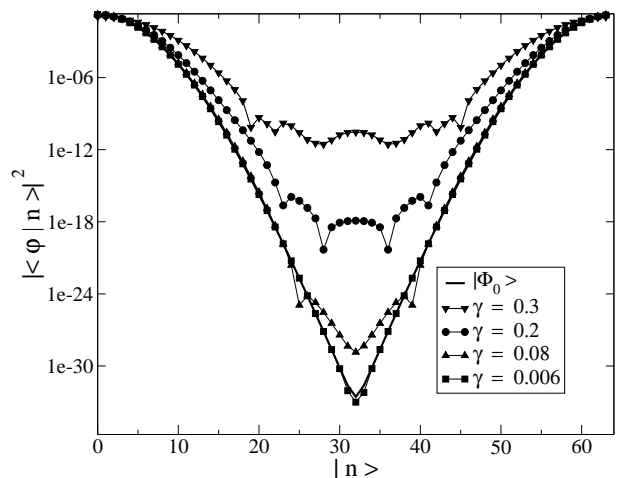


FIG. 6: Population (in the position basis) of the eigenstates of the Harper Hamiltonian and the Harper kicked map,  $\mathcal{U}(\gamma)$ , as a function of  $\gamma$ . We can appreciate that for the smallest values of  $\gamma$  these states are almost identical ( $N = 64$ ).

## B. Algorithm for phase estimation

As the phase estimation algorithm [20, 21, 22], is an essential part of our construction we briefly review its operation. The circuit is reproduced in Figure 7. Its operation in the phase estimation mode requires that an eigenstate of  $\mathcal{U}(\gamma)$  be supplied to the lower register. Then a measurement performed in the upper registers yields a rational approximation to the eigenphase, which improves as the size of the upper register increases. Here we are more interested in the use of the circuit as a filter in which case a state approximating an eigenstate is fed to the lower register. If this state is expanded as  $|\Psi\rangle = \sum_{\alpha} c_{\alpha} |u_{\alpha}\rangle$  the measurement in the upper register yields a distribution of phases with probabilities proportional to  $|c_{\alpha}|^2$ . Furthermore, if the number of qubits in the first register is such that the value of the phase can be exactly determined, then the final state of the second register is the eigenstate corresponding to that phase. Thus, it is clear that if the initial state  $|\Psi\rangle$  is near  $|\Phi_0\rangle$ , the application of this circuit would provide us with the desired state with high probability (see below).

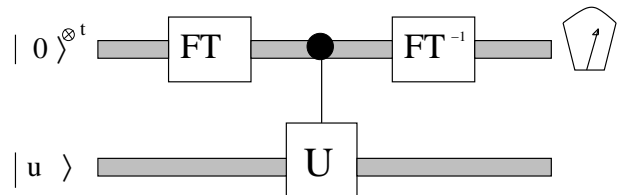


FIG. 7: The circuit for the phase estimation algorithm. When the state of the lower register is an eigenstate of  $U$ , the measurement of the upper register reveals an  $t$ -bit approximation to the corresponding eigenphase.

However, the typical situation is when the number of

qubits in the first register only allows us to make an approximation to the real value of the phase. Thus, if the system has  $n$  qubits and the number of qubits in the first register is

$$t = n + \log_2 \left[ 2 + \frac{1}{2\epsilon} \right], \quad (22)$$

the phase estimation algorithm gives an approximation to the phase corresponding to the eigenstate  $|u\rangle$ , with probability bounded by

$$p_u = |c_u|^2 (1 - \epsilon). \quad (23)$$

This clearly differs from the ideal case, since now we do not obtain the exact value of the phase. Therefore the above probability corresponds to the measurement of an integer  $k$  such that  $\frac{k}{2^t}$  is the best  $t$ -bit estimate to  $\varphi$  (with an error bounded by  $|2^{t-n} - 1|$ ). After the measurement, the state of the second register will be a linear combination of all the eigenstates of  $U$  that is close to the corresponding eigenstate (see below).

### C. Algorithm for the generation of coherent states

As mentioned above, the algorithm for the preparation of coherent states consists of the application of the phase estimation algorithm to filter an initial state (which should be itself a well localized state near the origin of phase space). We will now describe in detail the two necessary ingredients for the efficient implementation of the algorithm: i) the preparation of the initial state and, ii) the efficient implementation of the  $\text{ctrl-}\mathcal{U}^j(\gamma)$  gates, required for the phase estimation to be applicable.

#### 1. Initial state preparation

This is indeed the simplest part of the algorithm. In fact, an easily preparable candidate for the initial state is what we could denote as a “square state”, defined as an equally weighted superposition of the first  $\sqrt{N}$  states of the computational basis:

$$|\Psi_0\rangle = \frac{1}{w^{1/2}} \sum_{q=0}^{w-1} \left| \frac{w}{2} - q \right\rangle \pmod{N}, \quad (24)$$

where  $N$  is the Hilbert space dimension and  $w = \lceil \sqrt{N} \rceil$ . This state is strictly localized in position in a region of width  $w$  around the origin but, because of diffraction, is only partially localized in momentum. This can be seen by analyzing its Wigner representation shown in Figure 8. The important features of this state are that it has strong overlap with a coherent state localized at the origin of phase space (which is our target state). In the limit of large  $N$ , the overlap tends to a value of 0.94. Also, it is simple to show that the square state can be efficiently

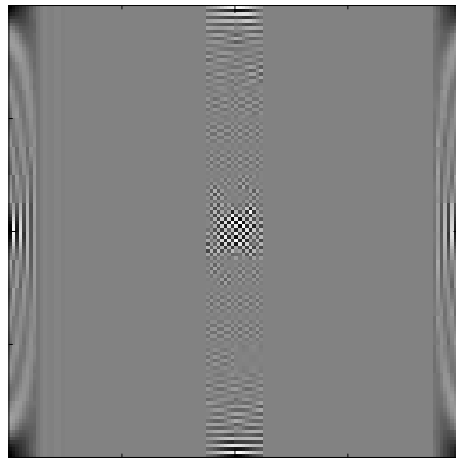


FIG. 8: The Wigner function of a square state. The state is located in position and partially localized in momentum ( $N=64$ ). Horizontal (vertical) axis corresponds to position (momentum) basis. The color convention is such that positive (negative) values of the Wigner function correspond to black (white) regions.

prepared: Starting from  $|0\rangle^{\otimes n}$  we simply need to apply Hadamard gates to the  $n/2$  least significant qubits we obtain a state centered at the phase space point  $(w/2, 0)$ . Centering the state at the origin requires a shift, which can be implemented efficiently.

#### 2. Efficient implementation of the $\text{ctrl-}\mathcal{U}^j(\gamma)$ gates

The phase estimation algorithm requires that the powers of the operator  $\mathcal{U}(\gamma)$  be implemented efficiently. This is in general not the case. However, we can get around this problem by using the fact that the Harper map has a well defined semi-classical limit. This allows us to perform its iteration by using a reliable semi-classical approximation. Thus, for  $\gamma \ll 1$  (and for  $N$  large) the powers needed can be approximated as follows:

$$\mathcal{U}^{2^t}(\gamma) \simeq \mathcal{U}(2^t \gamma). \quad (25)$$

This approximation also relies on the assumption that the initial state is localized in a region of the phase space where the map is regular (this is satisfied by the square state). If this approximation is valid, then the powers of the unitary operator can be implemented efficiently using the same quantum networks required to implement the operator itself (to implement a power of  $U$  we simply use a different parameter  $\gamma$ ). This approach has a clear limitation: Each power increases the value of  $\gamma$  and for large values of  $\gamma$  the map ceases to be integrable. In such case, its spectral properties become very different from those of the Harper Hamiltonian. Our goal then is to propagate the map for a time long enough to resolve the ground state from its neighbors without violating the approximation (25). These two issues (evolving accurately and resolving the spectrum) should be studied jointly.

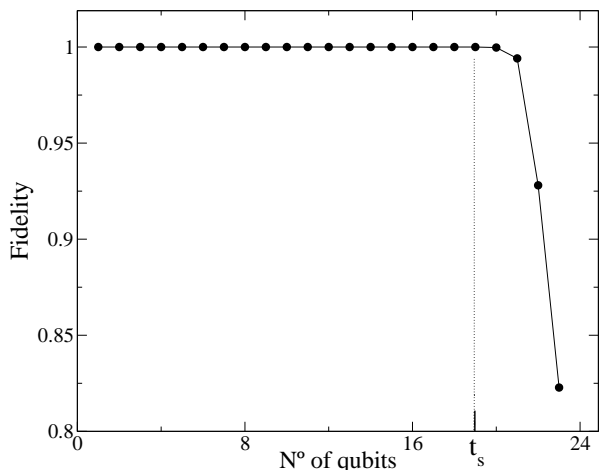


FIG. 9: The fidelity (overlap between the state evolved with the exact and approximated unitary operators) as a function of the number of qubits in the first register.  $2^{t_s}$  defines the maximum time for which (25) is valid.

But to make our presentation clear we can first analyze them separately.

To examine the accuracy of the approximate evolution we can study the fidelity, defined as the absolute value of the overlap between the square state propagated with the exact and approximate evolution (i.e.  $F = \sqrt{|\langle \psi_{exact} | \psi_{approx} \rangle|}$ ). In Figure 9 we plot this as a function of the number of qubits in the first register. We find that the fidelity remains close to unity up to a sharply defined time  $T_s$  ( $T_s = 2^{t_s}$ ), after which it drops abruptly. This time,  $T_s$ , defines the allowed number of iterations of the unitary compatible with a given accuracy. Therefore, it sets a bound to the maximum number of qubits we can include in the first register of the phase estimation algorithm for the semi-classical approximation to remain valid.

To analyze the resolution required to resolve the spectrum of the unitary operator we should consider the minimum difference between neighboring eigenphases of  $U(\gamma)$  (denoted as  $\Delta\varphi$ ). This quantity determines the minimum number of qubits in the first register, needed to resolve the ground state. Thus, for this purpose, we would need a number of qubits  $n$  which should be at least equal to

$$n = \log_2\left(\frac{1}{\Delta\varphi}\right). \quad (26)$$

An important question is how does this number scales with the dimension of the Hilbert space of the system. This can be determined by analyzing the dependence of  $\Delta\varphi$  with  $\gamma$  and  $N$ . This is done in Figure 10 where we show that the phase difference has a linear dependence with  $\gamma$ , at least for values of  $N$  and  $\gamma$  such that  $N\gamma < 0.6$ . Therefore, the number of qubits required to resolve the spectrum will scale logarithmically with the dimensionality of the system's Hilbert space.

As mentioned above, the behavior of the fidelity as a

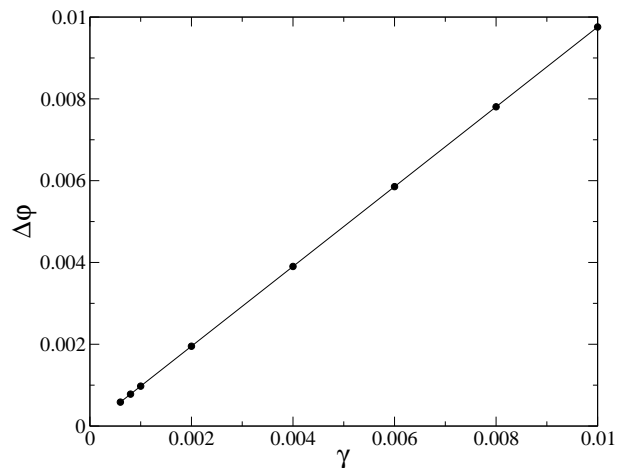


FIG. 10: Dependence of the phase difference  $\Delta\varphi$  with  $\gamma$ . A linear dependence is found for values of the Hilbert space dimension  $N$  such that  $N\gamma < 0.6$ .

function of the parameter  $\gamma$  should be analyzed jointly with the minimum number of qubits needed in the first register, to achieve the required spectral resolution according to eq. (26). In Figure 11 we display the curves coming from each of these requirements. To achieve high enough fidelity the value of  $\gamma$  and of the number of qubits in the first register must be below the lower curve. On the one hand to achieve the required spectral resolution one needs the value of  $\gamma$  and the number of qubits to lie above the second curve. This seem to be a problem, but can be easily solved taking into account the following observations. Thus, we notice that: i) the two lines are approximately parallel (for all values of  $N$ , as long as  $N\gamma < 0.6$ ) and ii) the two parallel lines are simply shifted away from each other by about three qubits. Hence, the semi-classical approximation can be used up to a power of  $U(\gamma)$  given by  $U(\gamma)^{2^{n-4}}$  with  $n = \log_2(\frac{1}{\Delta\varphi})$ . To iterate the map further, as required to achieve enough spectral resolution we can apply the remaining powers of  $U(\gamma)$  as products of its precedents (which were implemented using the semi-classical approximation). As the distance between curves is fixed, we would only need to use this trick a fixed ( $N$ -independent) number of times. Doing this, it is possible to achieve the required accuracy and spectral resolution simultaneously.

It is worth mentioning that the precision needed to resolve the ground state is not the only condition that imposes a lower bound on the number of qubits of the first register. Thus, in principle if we want to get the desired coherent state with a reasonable probability we need the number of qubits to obey the relation fixed by equation (23). Suppose that we impose a value of  $\epsilon = 1/4$ , which corresponds to a probability for preparing the right coherent state of about  $p_0 = 0.70$  (this is computed taking into account that the initial square state is such that  $|c_0|^2 = 0.94$ ). For this value of  $\epsilon$ , equation (23) implies that the first register should have at least two more qubits

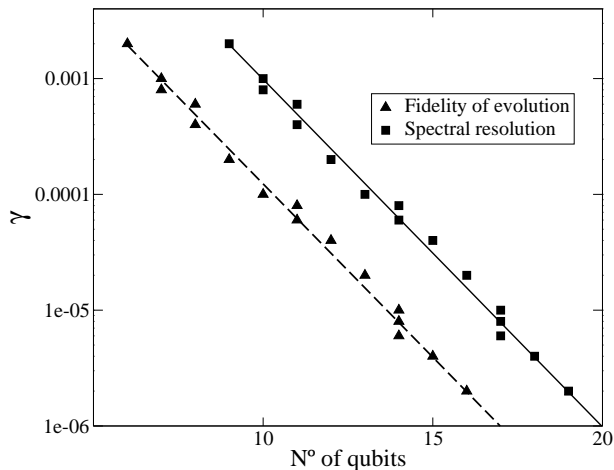


FIG. 11: Dependence of the parameter  $\gamma$  as a function of the number of qubits in the first register. The dashed line represents the condition of high fidelity in the evolution (the allowed parameter region lies below this curve). The solid line corresponds to the condition of good spectral resolution (the allowed parameter region lies above that curve). The two lines are shifted from each other by about three qubits.

than the system's register. This is a lower bound for the dimension of the first register.

### 3. Final remarks on the preparation of coherent states

In summary, the algorithm to prepare a coherent state consists of the following steps: i) preparation of a “square” state, ii) selection of the parameter  $\gamma$  for the evolution operator and the corresponding determination of the number of qubits to be used in the first register of the phase estimation algorithm, iii) run the phase estimation algorithm efficiently implementing the powers of the operator  $U(\gamma)$  in an approximate way, iv) from the peaked distribution of results for the phase, we discover the one associated with the coherent state, when this phase is detected the desired coherent state has been prepared in the system's register, v) after obtaining a coherent state centered at the origin, one can translate it to any point of the phase space using phase space displacement operator, which can be efficiently implemented as in the circuit of Figure 1.

To see the algorithm in action we performed a few numerical simulations. In Figures 12 we show the Wigner function of four of the quantum states of the system's register that fall under the peak of the probability distribution for the first register (we used  $N = 64$  and showed in Figure 13 the probability distribution for the same states in the computational basis). It is clear that any of such states is a good approximation to a coherent state (the fact that this stage of the algorithm works as a filter can be appreciated by comparing the initial square state shown in Figure 8 and those shown in Figure 12).

In Figure 14 we show how the approximation can be im-

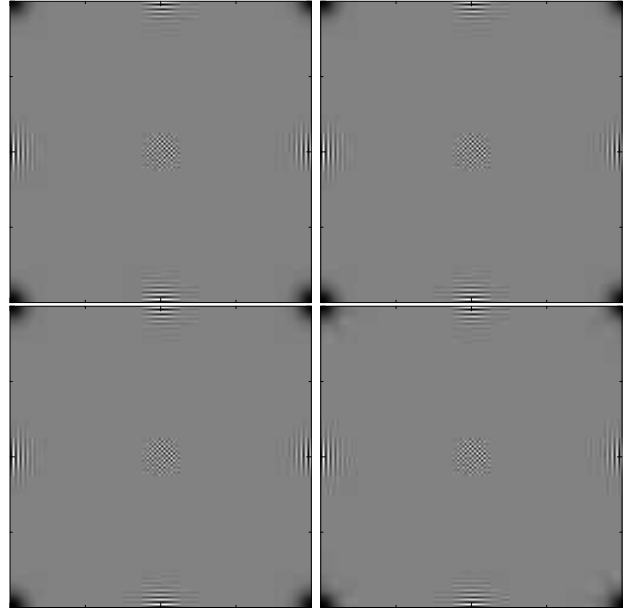


FIG. 12: Wigner function for four of the quantum states of the system's register that are generated by the phase estimation algorithm when the detected value of the first register falls in the peak of the probability distribution. Horizontal (vertical) axis corresponds to position (momentum) basis. Labeling these states from left to right and from top to bottom as a), b), c) and d), we can see in Figure 13 their representation in the computational basis.

proved even further by various means. In fact, we could include several stages of filtering each one of which would considerably improve the quality of the final state.

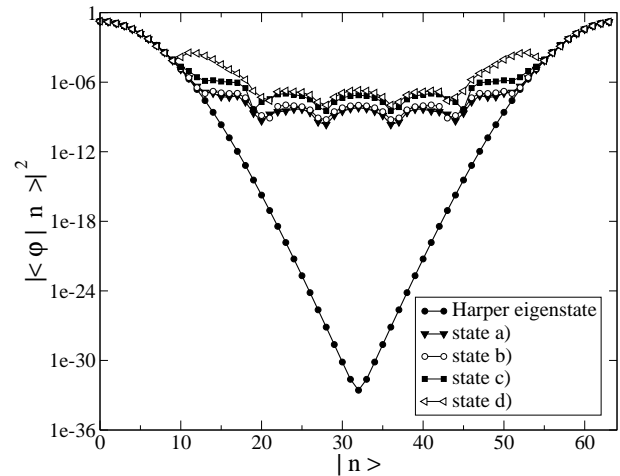


FIG. 13: Probability distribution in the computational basis for four of the quantum states of the system's register that are prepared when the detected value of the first register falls in the peak of the distribution. The Wigner function of such states is shown in Figure 12.



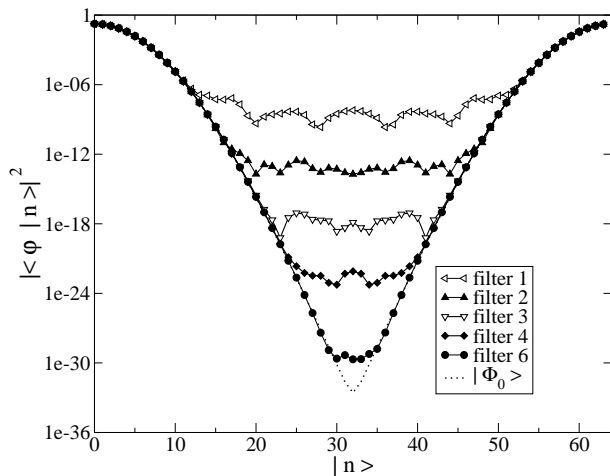


FIG. 14: Probability distribution in the computational basis for the states produced after different number of iterations of the filtering algorithm. Each iteration improves the quality of the state, which becomes closer to a true coherent state.

## VI. CONCLUSIONS

In this paper we presented various algorithms to evaluate several phase space distributions of arbitrary states. These methods allow, in principle, to perform phase space tomography in an efficient manner. The efficiency

of the circuits is based on the fact that operations such as phase space translations, reflections and the Fourier transform are efficiently implementable. For the case of Wigner and Kirkwood distributions, the efficiency is solely based on this fact (however, it is worth pointing out that, contrary to what happens with the Wigner and Husimi distributions, the evaluation of a typical value of the Kirkwood distribution of a pure state would require exponential precision due to the factor of  $N$  absent in (11) as compared with (3)). The evaluation of the Husimi distribution requires the use of a subroutine preparing coherent states. We presented a method achieving this goal, which consists of a variation of the phase estimation algorithm with an appropriately chosen initial state. In this case the efficiency requires not only a good guess for the initial state (which is indeed easily done) but also the possibility of efficiently implementing powers of the unitary map whose eigenstate is close to a coherent state. In our case, this can be done by using a semi-classical approximation for this operator.

## Acknowledgments

This work was partially supported with grants from Ubacyt, Anpcyt 03-9000, Conicet and Fundación Antorchas. JPP and AJR were also partially supported by a grant from NSA.

- 
- [1] N. L. Balazs and B. K. Jennings, *Phys. Rep.* **104**, 347 (1984).
  - [2] M. Hillery, R. F. O'Connell, M.O.Scully, E. P. Wigner, *Phys. Rep.* **106**, 121 (1984).
  - [3] W. K. Wootters, *Ann. Phys. NY* **176**, 1 (1987).
  - [4] U. Leonhardt, *Phys. Rev. Lett.* **74**, 4101 (1995); *Phys. Rev. A* **53**, 2998 (1996).
  - [5] J. H. Hannay and M. V. Berry, *Physica D* **1**, 267 (1980).
  - [6] A. Rivas and A. M. Ozorio de Almeida, *Ann. Phys. (San Diego)* **276**, 223 (1999).
  - [7] J. P. Paz, *Phys. Rev. A* **65**, 062311 (2002).
  - [8] M. Koniorczyk, V. Buzek and J. Janszky, *Phys. Rev. A* **64**, 034301 (2001).
  - [9] C. Miquel, J.P.Paz, M. Saraceno, *Phys. Rev. A* **65**, 62309 (2002).
  - [10] G. M. D'Ariano and P. Lo Presti, *Phys. Rev. Lett.* **86** 4195 (2001).
  - [11] C. Miquel, J. P. Paz, M. Saraceno, E. Knill, R. Laflamme, C. Negrevergne, *Nature* **418**, 59-62 (2002).
  - [12] see, for example, M. Dusek and V. Buzek, *Phys. Rev. A* **66**, 0022112 (2002); J. Fiurasek, M. Dusek and R. Filip, *Phys. Rev. Lett.* **89**, 190401 (2002).
  - [13] J. P. Paz and A. Roncaglia, *quant-ph/0306143* (2003).
  - [14] J. G. Kirkwood, *Phys. Rev.* **44**, 31-37 (1933).
  - [15] B. Georgeot and D. L. Shepelyansky, *Phys. Rev. Lett.* **86**, 2890-2893 (2001).
  - [16] M. Saraceno, *Ann. Phys.* **199**, 37-60 (1990).
  - [17] A. K. Ekert, C. M. Alves, D. K. L. Oi, M. Horodecki, P. Horodecki, L. C. Kwok, *Phys. Rev. Lett.* **88**, 217901 (2002).
  - [18] M. Hendrych, M. Dusek, J. Fiurasek, *Phys. Lett. A* **310**, 95 (2003).
  - [19] P. Leboeuf and A. Voros, *J. Phys. A* **23**, 1765 (1990).
  - [20] M. Nielsen and I. L. Chuang, *Quantum Computation and Quantum Information*, Cambridge (2000).
  - [21] R. Cleve, A. Ekert, C. Macchiavello and M. Mosca, *Proc. R. Soc. Lond* **454**, 339 (1996).
  - [22] D. S. Abrams and S. Lloyd, *Phys. Rev. Lett.* **83**, 5162-5165 (1999).